REGULAR ARTICLE

blood advances

Noncanonical type 2B von Willebrand disease associated with mutations in the VWF D′D3 and D4 domains

Monica Sacco,[1,*] Stefano Lancellotti,[2,*] Mattia Ferrarese,[3] Francesco Bernardi,[3] Mirko Pinotti,[3] Maira Tardugno,[1] Erica De Candia,[1,2] Leonardo Di Gennaro,[2] Maria Basso,[2] Betti Giusti,[4,5] Massimiliano Papi,[6] Giordano Perini,[6] Giancarlo Castaman,[7,†] and Raimondo De Cristofaro[1,2,†]

[1]Dipartimento di Medicina e Chirurgia Traslazionale, Facoltà di Medicina e Chirurgia Agostino Gemelli, Università Cattolica S. Cuore, Rome, Italy; [2]Servizio Malattie Emorragiche e Trombotiche, Fondazione Policlinico Universitario A. Gemelli, Istituto di Ricovero e Cura a Carattere Scientifico (IRCCS), Rome, Italy; [3]Dipartimento di Scienze della Vita e Biotecnologie, Università di Ferrara, Ferrara, Italy; [4]Dipartimento di Medicina Sperimentale e Clinica, Università di Firenze, Florence, Italy; [5]Laboratorio Genetico Molecolare Avanzato, Struttura Operativa Dipartimentale (SOD) Malattie Aterotrombotiche, Azienda Ospedaliero-Universitaria Careggi, Florence, Italy; [6]Dipartimento di Neuroscienze, Facoltà di Medicina e Chirurgia Agostino Gemelli, Università Cattolica S. Cuore, Rome, Italy; and [7]Centro Malattie Emorragiche e della Coagulazione, Dipartimento di Oncologia, Ospedale Universitario Careggi, Florence, Italy

Key Points

- The heterozygous *in cis* mutations R924Q/A2178S in a 55-year-old man caused a laboratory phenotype resembling a type 2B VWD.
- Mutations were identified in the D′D3 and D4 domains; thus, type 2B VWD can be generated not only by typical mutations in the A1 domain.

We observed a 55-year-old Italian man who presented with mucosal and cutaneous bleeding. Results of his blood analysis showed low levels of von Willebrand factor (VWF) antigen and VWF activity (both VWF ristocetin cofactor and VWF collagen binding), mild thrombocytopenia, increased ristocetin-induced platelet aggregation, and a deficiency of high-molecular-weight multimers, all typical phenotypic hallmarks of type 2B von Willebrand disease (VWD). The analysis of the *VWF* gene sequence revealed heterozygous *in cis* mutations: (1) *c.2771G>A* and (2) *c.6532G>T* substitutions in the exons 21 and 37, respectively. The first mutation causes the substitution of an Arg residue with a Gln at position 924, in the D′D3 domain. The second mutation causes an Ala to Ser substitution at position 2178 in the D4 domain. The patient's daughter did not present the same fatherly mutations but showed only the heterozygous polymorphic *c.3379C>T* mutation in exon 25 of the VWF gene causing the p.P1127S substitution, inherited from her mother. The in vitro expression of the heterozygous *in cis VWF* mutant rVWFWT/rVWF924Q-2178S confirmed and recapitulated the ex vivo VWF findings. Molecular modeling showed that these *in cis* mutations stabilize a partially stretched and open conformation of the VWF monomer. Transmission electron microscopy and atomic force microscopy showed in the heterozygous recombinant form rVWFWT/rVWF924Q-2178S a stretched conformation, forming strings even under static conditions. Thus, the heterozygous *in cis* mutations 924Q/2178S promote conformational transitions in the VWF molecule, causing a type 2B–like VWD phenotype, despite the absence of typical mutations in the A1 domain of VWF.

Introduction

von Willebrand factor (VWF) is a large multimeric glycoprotein mediating platelet adhesion to the damaged vessel wall under conditions of high shear stress.[1] The *VWF* gene, localized on chromosome 12, spans 178 kb and contains 52 exons. It is transcribed into an 8.8-kb messenger RNA, which encodes a 2813-aa precursor (pre-pro-VWF) consisting of a 22-aa signal peptide, a 741-aa propeptide,

Submitted 13 May 2020; accepted 22 June 2020; published online 28 July 2020. DOI 10.1182/bloodadvances.2020002334.

*M.S. and S.L. contributed equally to this study.

†G.C. and R.D.C. are joint senior authors.

Data-sharing requests may be e-mailed to the corresponding author, Raimondo De Cristofaro, at raimondo.decristofaro@unicatt.it.

The online version of this article contains a data supplement.

and a 2050-aa mature subunit.[2-4] The VWF mature subunit is composed of 4 repetitive domains designated A to D and arranged in the sequence D′-D3-A1-A2-A3-D4-C1-C2-C3-C4-C5-C6-CK.[5] The von Willebrand disease (VWD) is the most common and largely heterogeneous inherited bleeding disorder in humans, characterized by quantitative and/or qualitative defects of VWF.[6] The classification of congenital VWD is based on both clinical and laboratory findings according to the recommendations of the VWF Scientific Standardization Committee (VWF-SSC) of the International Society on Thrombosis and Haemostasis (ISTH).[7] Type 2 VWD is characterized by qualitative VWF abnormalities causing different functional defects.[7] In type 2B VWD, gain-of-function missense mutations in the VWF A1 domain favor interaction with both platelet glycoprotein Ib (GpIb) receptors and ADAMTS-13, with the consequent loss of the high- and intermediate-molecular-weight multimers.[8] Several type 2 VWD forms derive from compound heterozygous mutations that give rise to complex clinical and laboratory phenotypes.[9-12] In these complex cases, the ISTH VWD classification cannot clearly distinguish between the pronounced variants of type 1, 2M, and 2A (IIE) VWD, particularly when VWF levels are below 20 U/dL.[13] In this study, we analyzed a novel example of a complex genetic mutation. We report here 2 heterozygous *in cis* mutations (p.R924Q/p.A2178S) associated with a complex phenotype, whose genetic cause cannot be firmly assigned to any of the canonical forms of VWD.

Materials and methods

Patient

The propositus, an Italian man born in 1964, was observed for the first time in 2015 in our hospital during a clinical visit for severe bleeding (fall of hemoglobin [Hb] level = 3 g/dL in 2 days) due to a colon endoscopic polypectomy performed 3 days before without any antihemorrhagic prophylaxis. He did not report any family history of bleeding. Instead, his anamnesis reported a lifelong history of mild/trivial spontaneous bleeding (epistaxis, repeated gastrointestinal bleeding, and easy bruising), severe bleeding after a tonsillectomy at 5 years of age, when his hemorrhagic disorder was not yet diagnosed. At our center, he showed a bleeding time (Ivy test) >20 minutes (normal, <7 minutes). His ISTH Bleeding Assessment Tool (BAT) score was 7.[14] This patient was diagnosed in 2010 in another hospital as having a type 1 VWD. However, upon IV infusion of desmopressin, we observed no significant elevation of VWF level. In 2017, when a second colon polypectomy was performed and a diagnosis of type 2 VWD was established in our center, he successfully received VWF factor concentrate for the hemostatic challenge. His daughter did not show any menorrhagia and hemorrhagic disorder, except for a large hematoma of the thigh, which appeared after trauma of moderate intensity.

Measurements of VWF-related parameters

VWF antigen (VWF:Ag) and VWF ristocetin cofactor (VWF:RCo) were measured by chemiluminescence assays (ACL Acustar; Instrumentation Laboratory, Werfen Group, Milan, Italy).[15,16] Factor VIII (FVIII) activity was measured using a chromogenic assay (Instrumentation Laboratory, Werfen Group). FVIII binding to immobilized VWF was performed with the commercially available Asserachrom VWF:VIIIB assay (Stago, Asnières, France).[17] A VWF collagen-binding (VWF:CB) assay was performed using the Asserachrom VWF:CB assay (Stago, Asnières, France) using human type III collagen. The presence of anti-VWF antibodies was investigated first with the Bethesda assay using the Acustar VWF:RCo and thereafter confirmed with a previously detailed enzyme-linked immunosorbent assay method.[18] VWF propeptide (VWFpp) was measured by an enzyme-linked immunosorbent assay (Sanquin, Amsterdam, The Netherlands), as previously detailed.[19] The activity of ADAMTS-13 was measured by a fluorescence resonance energy transfer assay, as previously described.[20]

Electrophoresis of VWF multimers

The VWF multimer pattern (VWFm) was studied under low- (0.8% to 1.5% agarose) and high-resolution (0.8% to 2.5% agarose) conditions with sodium dodecyl sulfate (SDS)–agarose gel electrophoresis, as previously reported.[21]

Platelet-aggregation studies

Platelet-aggregation studies were performed with an AggRAM platelet aggregometer (Helena Biosciences) using 2 to 10 μM adenosine 5′-diphosphate, 10 μg/mL collagen, and 0.3 to 1.2 mg/mL ristocetin (Helena Biosciences). The platelet-aggregation assays were performed using both plasma of the patients and the recombinant forms of VWF, used in all cases at a concentration of ≈2 μg/mL. Mixing tests in aggregometry assays was also carried out to exclude platelet-type VWD. Thus, gel-filtered platelets from both the patient and 5 healthy subjects were tested in crossover aggregometry assays with both normal platelet-poor plasma (PPP) obtained from the healthy subjects and with PPP from the patient.[22] The ristocetin-induced aggregation by the recombinant VWF forms was tested using gel-filtered platelets from healthy donors.

DDAVP test

IV infusions of 1-desamino-8-D-arginine vasopressin (DDAVP; 0.3 μg/kg body weight, diluted in 100 mL of saline) were administered under medical supervision. Blood was withdrawn for VWF/FVIII analysis and cell blood count at baseline and 2 hours after the infusion ended.

Molecular genetics

Molecular genetic analysis of the *VWF* gene was performed for the propositus, his daughter, and his wife. Informed consent for the study was obtained according to the Declaration of Helsinki. Unfortunately, we could not collect blood from the patient's parents, as they were deceased. The paternity test was performed with the Power-Plex-16 kit (Promega Corp, Madison, WI) following the manufacturer's instructions. Analysis of the polymerase chain reaction products (3 μL) was carried out with the an 3100-Avant Genetic Analyzer (Applied Biosystems, Foster City, CA). The quality control followed the proficiency testing of International Society for Forensic Genetics Working Group (ISFG-WG) guidelines.[23] Genomic DNA was isolated from peripheral blood leukocytes using the QIAamp DNA Mini kit (Qiagen, Hilden, Germany). Sanger-sequencing procedures were carried out to validate the identified genetic variants. The specific primer sets were designed using the Primer3 algorithm (http://frodo.wi.mit.edu/primer3). Other experimental details are provided in supplemental Materials.

Expression and purification of recombinant WT and mutated forms of VWF

Expression vectors. The recombinant pSVH expression plasmid containing full-length complementary DNA (cDNA) encoding wild-type (WT) human VWF (pSVHVWFwt) has been described previously.[24] The VWF cassette enclosed by *Sac*I restriction sites was subcloned into the pCMV6 expression plasmid (pCMV6-*Sac*Iwt) to be further modified. VWFwt cDNA, obtained by restriction of pSVHVWFwt with *Eco*RI, was cloned into the pcDNA3 expression vector to generate the pcDNA3-VWFwt plasmid. Mutation R924Q was introduced into pSVHVWFwt plasmid with the QuickChange II XL Site-Directed Mutagenesis kit (Agilent Technologies, Santa Clara, CA) and the resulting mutated cDNA was verified by Sanger sequencing and cloned with *Eco*RI into pcDNA3 to obtain the pcDNA3-VWFR924Q vector. Mutation A2178S was introduced into pCMV6-*Sac*Iwt by site-directed mutagenesis. The resulting mutated cassette was sequenced and subcloned with *Sac*I into pSVHVWFwt or pSVHVWFR924Q plasmids. Finally, these mutated cDNAs were cloned with *Eco*RI into pcDNA3 to generate pcDNA3-VWFA2178S and pcDNA3-VWFR924Q/A2178S, respectively.

Cell culture. HEK293T cells were grown under sterile conditions and adherence in flasks containing Dulbecco modified Eagle medium supplemented with 10% fetal bovine serum, 4 mM L-glutamine, 125 IU/mL penicillin-G, and 125 ug/mL streptomycin. The cell culture was maintained at 37°C and 5% CO_2.

Transfection. HEK293T cells were transiently transfected using Lipofectamine 2000 (Invitrogen/Thermo Fisher Scientific, Waltham, MA) according to the manufacturer's instructions. Briefly, cells in a T75 flask at 80% of confluency were transfected in OptiMEM (Gibco/Thermo Fisher Scientific) with 12 μg of plasmid DNA. The medium was harvested 48 hours after transfection. With this procedure, the following constructs were produced: rVWFWT, heterozygous *in cis* mutant rVWFWT/rVWF924Q-2178S, homozygous rVWF924Q-2178S, heterozygous rVWFWT/rVWF2178S, and homozygous rVWF2178S.

Purification of recombinant VWF variants. Phenylmethylsulfonyl fluoride (100 μM) was added to collected media, which were centrifuged at 5000*g* for 5 minutes at 4°C and dialyzed against *N*-2-hydroxyethylpiperazine-*N*′-2-ethanesulfonic acid (HEPES) buffered saline overnight at 4°C. VWF variants were then purified by size-exclusion fast protein liquid chromatography (ÄKTA Pure Protein Purification System; GE Healthcare/Life Sciences), using a HiPrep 16/60 Sephacryl S-500 HR column (GE Healthcare/Life Sciences). The purified protein was aliquoted and rapidly stored at −80°C

Structural analysis of the missense VWFp.R924Q-A2178S mutant using molecular modeling

The heterozygous *in cis* missense mutations p.R924Q and p.A2178S identified in this VWF molecule are in 2 domains, whose crystal-based structures have only partly been resolved. X-ray crystal structures deposited in the Protein Data Bank (PDB) site are the D′D3 (S764-L1243), A1 (D1261-1468), A2 (M1495-H1674), and A3 domains (D1685-S1873) (PDB file identifiers "6N29," "1AUQ," "3GXB," and "1ATZ," respectively).

Table 1. Laboratory parameters of the patient

Parameter	Value	Value post-DDAVP	Normal values
Gene mutations	Het. *in cis* mutations c.2771G>A (exon 21) + c.6532G>T (exon 37)		
INR	0.95	—	0.8-1.2
aPTT, s	45.4	44.3	22-38
Fibrinogen, mg/dL	349	338	200-400
VWF:Ag, IU/dL	23.4	29	50-150
VWF:RCo, IU/dL	8.5	10	50-150
VWF:CBA, IU/dL	7.2	8	50-150
FVIII:C, IU/dL	28.2	33	50-150
VWFpp, %	63.4	—	50-120
VWF:RCo/VWF:Ag	0.36	0.34	0.75-1.25
VWF:CBA/VWF:Ag	0.31	0.28	0.75-1.2
VWFpp/VWF:Ag	2.7	—	0.75-1.25
FVIII/VWF:Ag	1.2	1.14	0.75-1.25
FVIII/VWF:binding, %	127.8	—	70-130
ADAMTS-13 act, U/dL	110.1	—	70-130
Platelets, $\times 10^9$/L	121-166	85	200-400
Hb, g/dL	8.1-15.1	—	12.5-15
Blood group*	A-Rh +Rh phenotype: ccDEe Kell/Cellano phenotype: kk	—	—

—, the measurement of the corresponding parameter was not performed; ADAMTS-13 act, ADAMTS-13 activity; aPTT, activated partial thromboplastin time; CBA, collagen-binding assay; FVIII:C, FVIII coagulant; Het., heterozygous; INR, international normalized ratio.

*Blood group of the daughter: A-Rh + - Rh phenotype: CcDee-Kell/Cellano: kk.

Thus, we decided to perform molecular modeling of the VWF sequence S764-V2191 using the I-TASSER threading modeling server (Iterative ThreadingASSEmbly Refinement) (http://zhanglab.ccmb.med.umich.edu/I-TASSER/).[25,26]

TEM analysis

Samples for transmission electron microscopy (TEM) were prepared by dialyzing for 24 hours at 4°C VWF variants for purification in 20 mM HEPES, 150 nM NaCl, pH 7.40. Proteins were concentrated up to 25 ng/mL. Salt crystals in the samples were eliminated with Zeba Desalt Spin Columns (Thermo Scientific). Subsequently, a small drop (10 μL) was dispersed on carbon-coated glow-discharged copper grids and stained with a small drop of 2% uranyl acetate before dehydration.

Atomic force microscopy

Atomic force microscopy (AFM) imaging was performed using a NanoWizard II (JPK Instruments, Berlin, Germany) in the contact operation mode. All samples were kept in an aqueous environment and at a controlled temperature (25°C) throughout the measurement procedure, as detailed elsewhere.[27] This approach was aimed at minimizing perturbations and artifacts due to salt crystallization following dehydration that could hide or modify the real particle structure.[28]

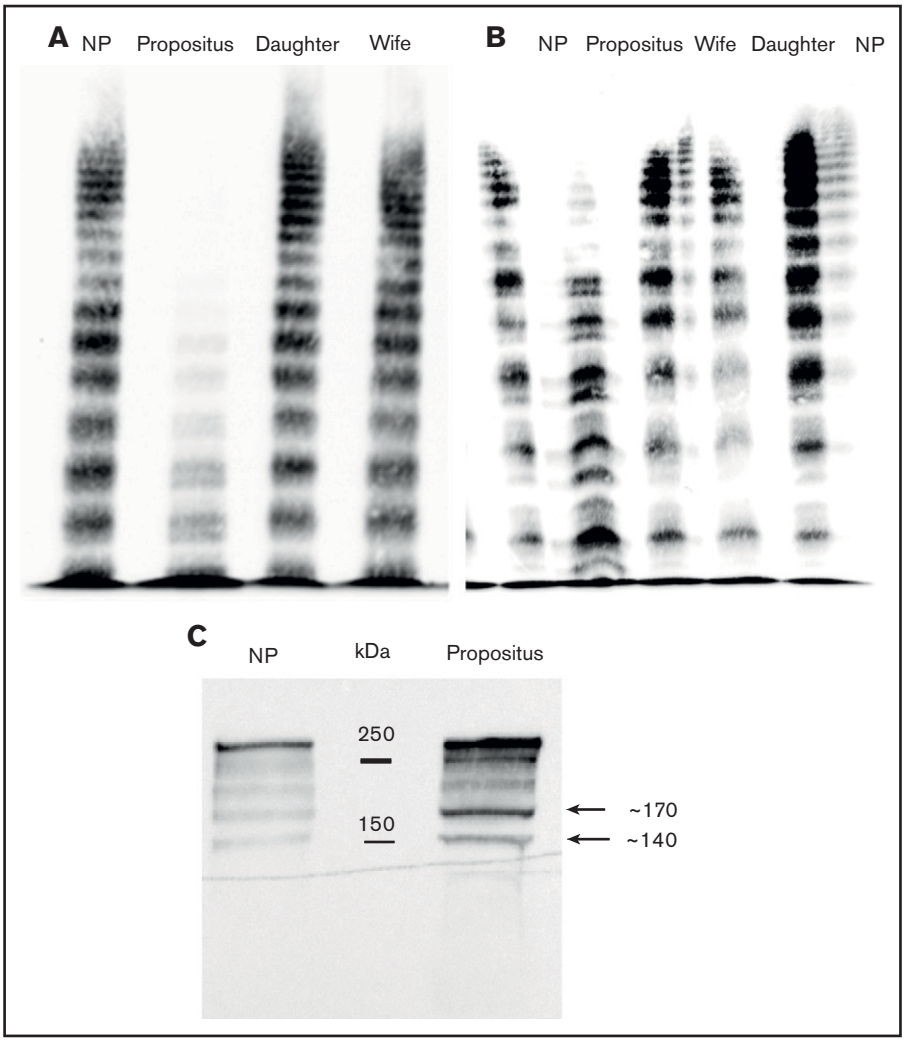

Figure 1. SDS-agarose and SDS-PAGE of VWF multimers. (A) SDS–agarose electrophoresis gels of VWFm in the patient, his wife, and daughter. The bands were detected with a ChemiDoc densitometer (Bio-Rad). (B) Discontinuous high-resolution (0.8% to 2.5%) SDS-agarose gel electrophoresis of VWFm from the same plasma sample. (C) Western blots of VWF samples of the patient reduced with phosphine (Bio-Rad) in precast SDS-PAGE (4% to 12%) gel using a Criterion apparatus (Bio-Rad).The arrows indicate VWF bands produced by the ADAMTS-13 proteolysis. NP, normal plasma.

Results

VWF-related parameters

The patient had a moderate reduction of VWF:Ag plasma levels, and a more pronounced reduction of VWF activity and VWF:CB plasma levels as listed in Table 1. As a consequence, the relative VWF:RCo/VWF:Ag and VWF:CB/VWF:Ag ratio values were markedly reduced. Anti-VWF antibodies were absent. These findings agreed with the multimer VWF analysis that showed a severe absence of both high- and intermediate-molecular-weight multimers (defined as the cumulative bands above the 10th band and between the seventh and 10th bands, respectively) as shown in Figure 1A. Moreover, the analysis of the high-resolution SDS–agarose gel electrophoresis showed an accumulation of small multimers and a stronger representation of the satellite bands of each oligomer (Figure 1B). SDS–polyacrylamide gel electrophoresis (PAGE) of the reduced VWF samples from the propositus showed, compared with normal plasma, increased representation of the 170- and 140-kDa bands, which are the products of the ADAMTS-13 activity (Figure 1C). The FVIII:C level was found proportional to the VWF:Ag level, resulting in an FVIII/VWF ratio of 1.2. FVIII-binding assays performed on plasma samples from the propositus demonstrated normal values, as shown in Table 1. We next explored whether the decreased VWF:RCo/VWF:Ag ratio of the propositus could be associated with accelerated peripheral clearance of high-molecular-weight multimers. To address this point, we measured plasma levels of VWFpp.[19] In the patient, the VWFpp/VWF:Ag ratio results were abnormally increased, being equal to 2.7 (normal median value, 0.85 [interquartile range, 0.75-1.25] in 10 healthy controls).

Characterization of genetic mutation

The analysis of the propositus' *VWF* gene sequence revealed 2 *in cis* heterozygous mutations: (1) the *c.2771G>A* substitution in exon 21 and (2) the *c.6532G>T* substitution in exon 37. The *c.2771G>A* change causes the substitution of an arginine residue with glutamine at position 924 (p.R924Q), in the D′D3 domain of the mature protein. Arg924 is implicated in the interaction with FVIII.[29] Although the effect of this mutation is highly debated in the literature,[30] some functional studies also indicate a capacity of the variant to alter VWF levels.[29,31] The variant is reported in the dbSNP database (http://www.ncbi.nlm.nih.gov/snp/), rs33978901, with a minor allele frequency in the European population ranging between 0.01 and 0.02, or in other studies as a polymorphic variant.

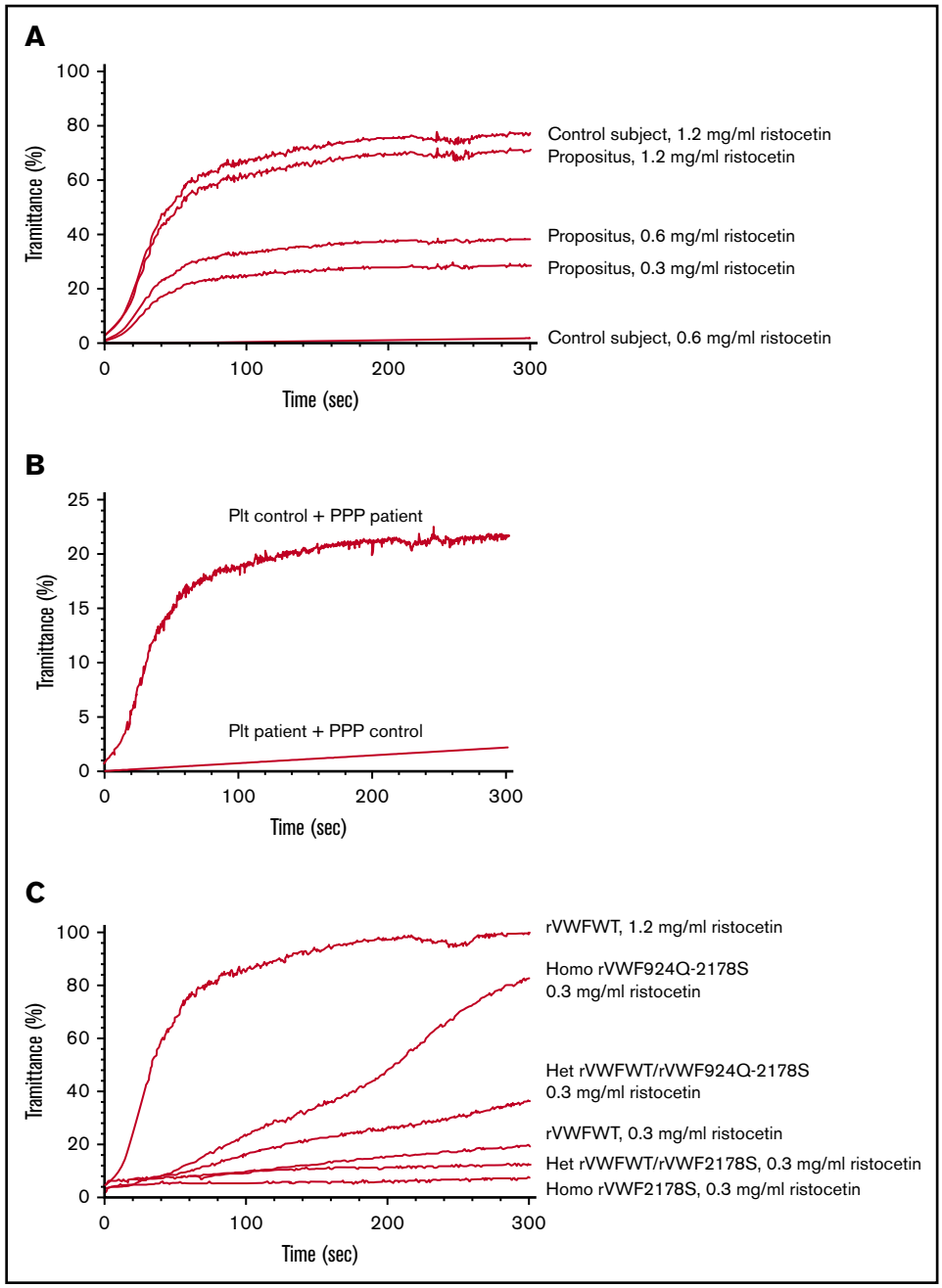

Figure 2. Ristocetin-induced platelet aggregation of the patient. (A) Ristocetin-induced platelet aggregation of the patient and age- and sex-matched healthy control subject. The concentration of ristocetin used in each test is indicated; in all cases, the VWF concentration was 20 IU/dL. (B) Crossover aggregometry assay using gel-filtered platelets from normal control (Plt ctrl, 140 000/μL) in the presence of the patient's PPP and platelets from the patient at the same count with PPP from normal control. The latter was used at the same VWF concentration present in the patient's plasma (2 μg/mL) by diluting it with plasma of a subject with type 3 VWD. Ristocetin was used at 0.6 mg/mL. (C) Ristocetin-induced aggregation of gel-filtered platelets from a healthy control subject tested with the recombinant VWF constructs indicated in the figure. In all cases, the VWF concentration was 20 IU/dL.

[32,33] The genetic variant c.6532G> T identified in exon 37 of the *VWF* gene causes the replacement of the alanine at position 2178 with a serine (p.A2178S). The variant is reported in the dbSNP database (http://www.ncbi.nlm.nih.gov/snp/), rs34230288, with a minor allele frequency in the European population of 0.02. This variant is tolerated in all of the in silico systems used. Unexpectedly, none of these mutations were found in his daughter. Thus, a paternity test was mandatory; the true paternity was confirmed with a Combined Paternity Index (CPI) $>299 \times 10^6$ and a paternity probability >99.99999%. The VWF genetic profiles of the patient, his daughter, and his wife as well as the result of the paternity test allowed us to conclude that the patient was affected by 2 heterozygous *in cis* mutations: p.R924Q/p.A2178S (Table 1).

Expression of recombinant VWF constructs

All of the recombinant VWF variants (rVWFWT, rVWFWT/rVWF 924Q-2178S, homozygous rVWF924Q-2178S, heterozygous rVWFWT/rVWF2178S, and homozygous rVWF2178S) were produced and secreted by HEK293T cells in good amounts and normal multimeric pattern (supplemental Figure 1).

Platelet aggregation

The platelet aggregation induced by adenosine 5′-diphosphate and collagen was normal (data not shown) but increased response to low-dose ristocetin was observed. Although the PPP contained a low VWF:Ag level (23 U/dL), a drastic increase of the platelet

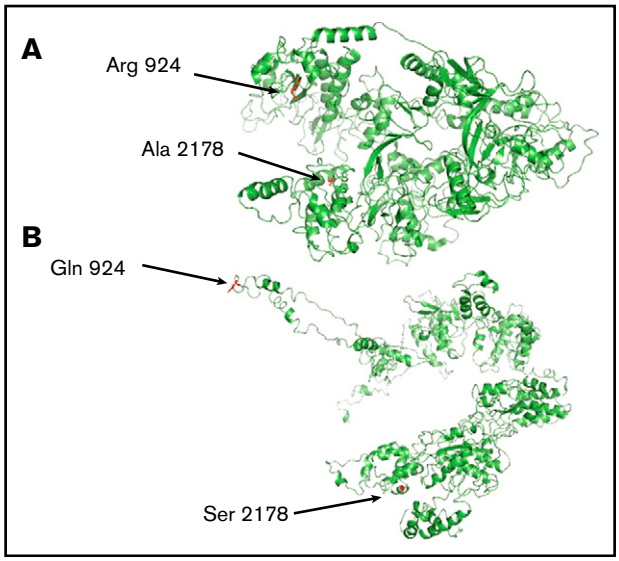

Figure 3. Prediction of the molecular structure. Prediction of the molecular structure of the VWF sequence 764-2191 for both the WT (A) and the double mutant p.R924Q and p.A2178S (B). Model joining was performed by constraining the intrachain disulfide bonds previously assigned with x-ray diffraction and biochemical studies.[5] The accuracy of the generated models was assessed with the ResQ program,[36] which checks the residue-specific local quality of the I-TASSER models. The ResQ algorithm analyzed and assessed the validity of several parameters: (a) the structural variations of Monte Carlo assembly simulations, (b) distance deviations of the templates detected by threading and structural alignment, (c) the threading alignment coverage, and (d) the consistency between the model and the sequence-based predictions of structural features. All structural analysis and image rendering were performed with the Pymol software (v. 2.3.3). The 2 models are shown in the same orientation. I-Tasser and ResQ were used to generate the models. R924, Q924, A2178, and S2178 are shown in red sticks. Pymol software was used to view and manipulate the generated PDB file.

aggregation was observed at low ristocetin concentration (0.3 mg/mL). In fact, platelet agglutination by 1.2, 0.6, 0.3 mg/mL ristocetin was equal to 71%, 40%, and 28%, respectively (Figure 2A). The crossover aggregometry experiments showed that platelets of the patient had a normal response to 1.2 mg/mL ristocetin but very low or no aggregation was recorded at 0.6 mg/mL ristocetin in the presence of PPP from normal subjects. At variance with this result, platelets from healthy controls showed an abnormally high aggregation when tested with PPP of the patients at 0.6 mg/dL ristocetin (Figure 2B). The recombinant WT and mutant VWF constructs were also tested in aggregometry experiments. Homozygous rVWF 924Q-2178S showed a maximum aggregation in the presence of 0.3 mg/mL ristocetin comparable to that elicited by 1.2 mg/mL rVWFWT (Figure 2C). At 0.3 mg/mL ristocetin, rVWF924Q-2178S showed an $\cong$32% maximum aggregation, whereas for rVWFWT, heterozygous rVWFWT/rVWF2178S, and homozygous rVWF2178S, aggregation was virtually absent (Figure 2C). The propositus did not respond to desmopressin. Indeed, 2 hours after infusion of desmopressin at a dose of 0.3 μg/kg body weight, he showed a very modest increase of VWF:Ag, VWF:RCo, and FVIII (Table 1), with transient thrombocytopenia (platelet count pre-DDAVP 159 $\times$ 10^9/L, post-DDAVP 85 $\times$ 10^9/L), associated with the formation of platelet clumps 2 hours after the infusion (data not shown).

ADAMTS-13 level and proteolyzed VWF fragments

Plasma ADAMTS-13 activity level values for the patient, as listed in Table 1, were normal. Hence, the increased presence of the proteolyzed VWF bands in the propositus' plasma (Figure 1C) was not produced by the enhanced activity of the enzyme but, rather, by a different susceptibility of VWF to the ADAMTS-13 activity.

Molecular modeling of the missense mutations p.R924Q and p.A2178S

I-TASSER was used to generate structure predictions for both the WT VWF monomer (sequence 764-2191) and the mutant bearing the point mutations p.R924Q and p.A2178S (Figure 3). The mean estimated template model (TM) and root-mean-square deviation (RMSD) score, calculated for the statistically best models, were equal to 0.94 and 3.85 Å, respectively, for the WT VWF form and 0.93 and 4.64 Å, respectively, for the heterozygous rVWFWT/rVWF 924Q-2178S form. These modeling results are largely consistent with the good results from the I-TASSER modeling in the previously reported Critical Assessment of Structure Prediction (CASP) experiments.[34,35] The ResQ program uses algorithms to predict the TM score and RMSD of the model relative to its native structure based on the predicted local distances, with the corresponding TM score and RMSD formula.[36] Estimated local quality and B factor for the residues of the WT and double mutant VWF constructs are reported in supplemental Tables 1 and 2. Notably, the change of polarity and charge of the 2 missense mutations caused a major conformational change in the global structure of the mutant compared with the WT monomer, as shown in Figure 3. The substitution of Arg924 with a Gln residue, for instance, causes a loss of several polar contacts between the side-chain atoms of Arg924 and Gly913, His916, and Lys843 (Figure 4A). The absence of these polar interactions likely contributes to partial opening of the compact assembly of β5-β12 strands in the D3 domain, as predicted by the modeling shown in Figure 3. Likewise, the polarity change due to the presence of the hydroxyl residue of S2178 causes a partial distortion of the α4 helix in the D4 domain (Figure 4B-C).

TEM

Electron micrographs of both rVWFWT and the heterozygous rVWFWT/rVWF 924Q-2178S are shown in Figure 5A-B. A significant difference was observed in the conformation of the WT and the mutant. The WT form was observed in a compact/globular configuration like a "ball of yarn" (Figure 5A), whereas the heterozygous rVWFWT/rVWF 924Q-2178S mutant was mainly present as fully extended bundles, occasionally approaching a length of 1000 nm but usually being $<$500 nm long and forming pieces of a net due to strings crossing (Figure 5B). In the TEM images, the fully folded conformers showed a diameter of the major axis ranging from 3 to 20 nm.

AFM

The images obtained with AFM under static conditions showed structural patterns of both the rVWFWT and the heterozygous rVWFWT/rVWF924Q-2178S constructs very similar to that obtained with TEM (Figure 5C-D). This is particularly relevant because in the TEM experiments, samples were dry; in the AFM experiments, the samples were hydrated. Despite the different hydration conditions, the presence of extended conformers of the

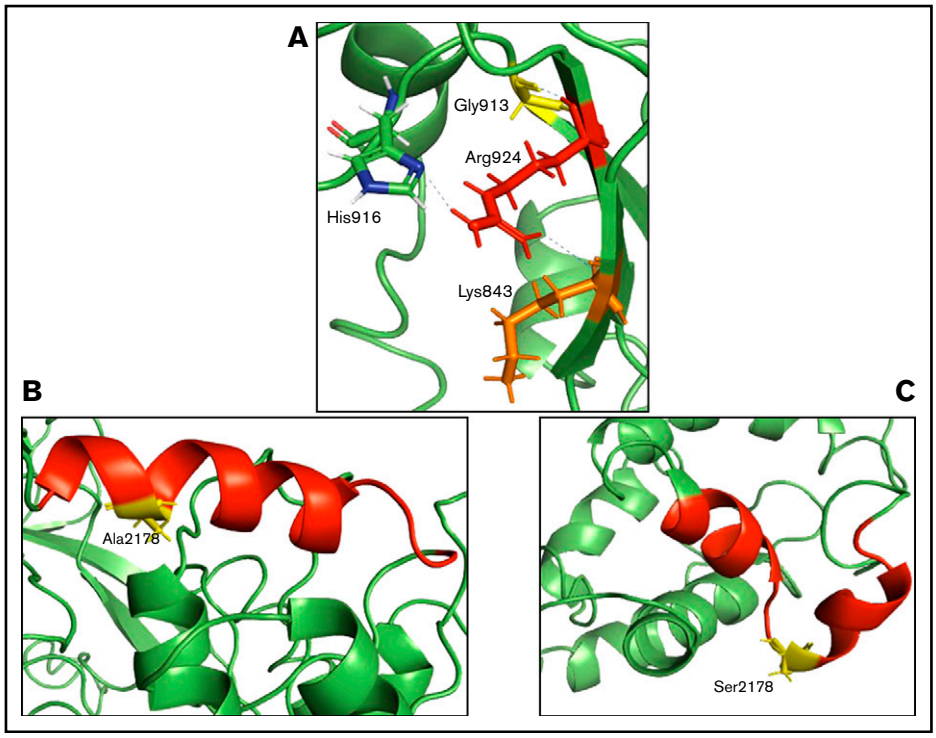

Figure 4. Details of the model of WT VWF and heterozygous *in cis* p.R924Q/p.A2178S (sequence Ser764-Val2191) obtained with the I-Tasser program. (A) Hydrogen bonds between the side chain of R924 with the side chains of surrounding residues in WT form. These bonds are completely lost in the heterozygous *in cis* mutant. The figure, prepared with the PyMol software, shows the polar interactions (dashed lines in yellow) of the side chain of Arg924 with surrounding amino acids. Structure of the α4 chain of the D4 domain (H2169-A2181 in the red cartoon with the side chain of A2178 in yellow sticks) of the WT VWF form (B) and in the heterozygous *in cis* p.R924Q/p.A2178S mutant (H2169-A2181 in the red cartoon with the side chain of S2178 in yellow sticks) (C). To assess the putative structural effect of the *in cis* heterozygous p.R924Q/p.A2178S mutations over the entire region from Ser764 to Val2191, also comprising part of the D4 domain (V1875-V2191),[5] we modeled this region on the I-TASSER threading modeling server (Iterative Threading ASSEmbly Refinement; http://zhanglab.ccmb.med.umich.edu/I-TASSER/).[25,26]

rVWFWT/rVWF 924Q-2178S construct were observed in the AFM analysis with similar dimensions (Figure 5C-D). In the mutant form, the AFM technique allowed a 3-dimensional (3D) analysis revealing a bundle height of ~27 nm (Figure 5D). This finding is likely explainable with overlapping strings forming a net through processes of molecular interstring aggregation. Furthermore, AFM was used in force-measuring experiments on a single molecule (Figure 6). In a typical stretching experiment, the force-extension curve shows a saw-tooth pattern, each peak corresponding to the unfolding of a single domain of the protein. The force-extension profile of a polymeric molecule like VWF is complex and cannot be fully interpreted.[37] However, the height of each force peak reflects the energetics of the mechanical stability of a protein's domain, whereas the distance between peaks measures the length of the protein region that is unfolded.[38] Figure 6A-B shows that the global profile and the peak height of the mutant VWF are very different (Figure 6B) from those of the WT form (Figure 6A). The saw-tooth pattern observed in the WT form, although having complex asymmetry characteristics, was almost completely lost in the mutant VWF. Moreover, the WT form has a median unfolding force of ~17 pN (Figure 6C), whereas the heterozygous rVWFWT/rVWF 924Q-2178S has an average unfolding force of ~7 pN (Figure 6D).

Discussion

We report here the first case of a type 2B VWD patient carrying mutations at the D′D3 and D4 VWF domains. From a simply phenotypic standpoint, we could assign this case to a canonical type 2B VWD, associated with gain-of-function missense mutations over the region comprising the amino acid 1266-1461 in the A1 domain of the VWF molecule.[21,39] The gain-of-function mutations in the type 2BVWD arise from the capacity of these VWF mutants to undergo an easier conformational transition under low shear forces from a globular to a stretched conformation. This change permits the interaction with platelet GpIb and ADAMTS-13.[21,40-43] The enhanced VWF-induced platelet aggregation causes their consumption, and accelerated proteolysis by ADAMTS-13 contributes to the loss of the high- and intermediate-molecular-weight multimers, as usually observed in type 2B VWD. This is in conformity with results obtained from electrophoretic studies of VWF multimers (Figure 1A-B) and the increase of the VWFpp/VWF:Ag ratio observed in our propositus. Based on phenotypic and laboratory findings of the propositus, we expected to find mutations in the VWF A1 domain to confirm a canonical type 2B VWD diagnosis. At variance with this hypothesis, we found heterozygous *in cis* mutations within the D′D3 and D4 domains. The former is usually invoked as the site of mutations responsible for the reduced VWF interaction with FVIII, found in the type 2N VWD.[44] However, in the propositus, the value of the FVIII/VWF ratio and the measured FVIII-VWF interaction were normal. Both TEM and AFM experiments clearly showed that, even under static conditions, the compound heterozygous VWF form is mainly composed of stretched conformers. The prevalence of extended conformers explains the

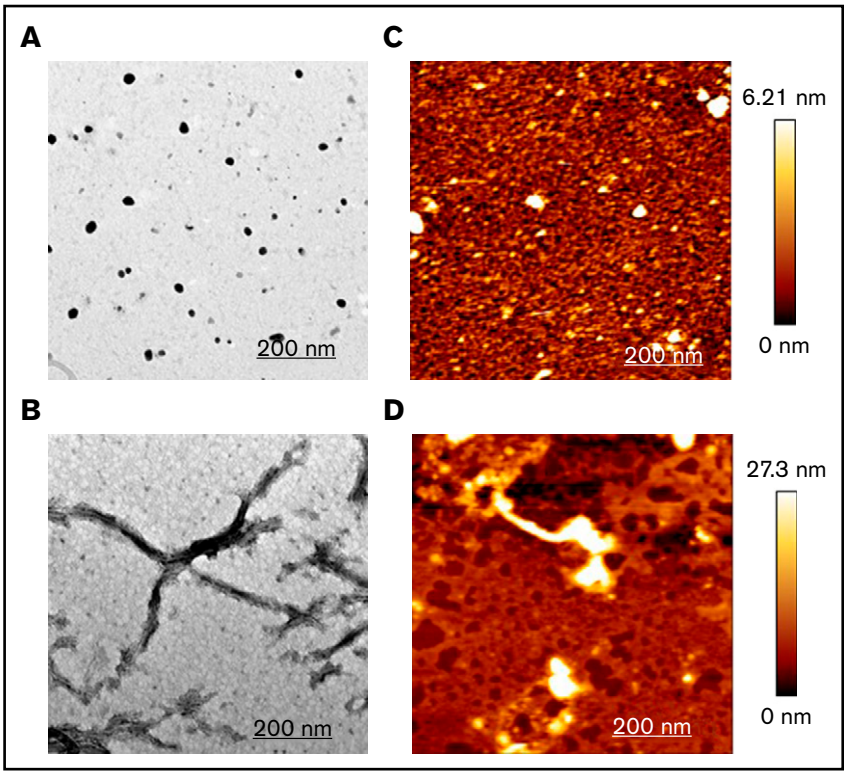

Figure 5. TEM analysis. TEM analysis of both the recombinant rVWFWT (A) and heterozygous *in cis* rVWFWT/rVWF924Q-2178S form (B) and images obtained with AFM of the recombinant WT (C) and mutant (D) VWF form. (A-B) The sample could adsorb on the carbon film for 5 minutes, and the sample excess was removed with filter paper. After staining with a 2% uranyl acetate solution for 30 seconds in the dark at room temperature, staining excess was also removed with filter paper and the grid washed with ultrapure water. Grids were then air-dried for 1 hour before observation at room temperature. TEM micrographs were collected, working with an acceleration voltage of 120 keV at a magnification of ×30 000 (Libra 120; Carl Zeiss Meditec, Jena, Germany). Notably, a great difference in the conformational state between the 2 forms can be observed. Even in the absence of shear stress, the conformation is globular for the WT VWF, whereas it is mainly unfolded for the mutant, which forms strains interacting each other. The samples were dry in the TEM method (tungsten-coated, brightfield-imaged), whereas they were (C-D) fully hydrated in the AFM experiment.

facilitated interaction with the platelet GpIb and ADAMTS-13. Altogether, these molecular abnormalities, although not involving mutations in the A1 domain, greatly resemble the laboratory findings of a canonical form of a type 2B VWD. Based on this scenario, the question arises regarding which mechanism is responsible for this apparently contradictory situation. We believe that the unexpected or apparent mismatches between the phenotypic manifestations and the localization of genetic mutations, observed in this case, stem from the structure and conformational equilibria, to which the VWF multimers are strongly subjected.[45-47] In this case, an early step of the VWF molecule maturation process, that is the dimerization, may be specifically affected by the heterozygous *in cis* mutations described herein. At the acidic pH present in the Golgi apparatus and Weibel-Palade bodies, the C terminus of ≅1350 aa of VWF zip up into an elongated conformer, resembling a dimeric bouquet, ~63 nm long.[48] The formation of this bouquet engages a rigid stem, the D4-C1-C2 domains, and a more flexible petal-like terminus, composed of the D′D3-A1-A2-A3 domains.[48] In the molecular "bouquet," the interaction between the coupled D4 domains of 2 different monomers drives their approach, facilitating the formation of disulfide bonds through cysteines in the CK domains. Thereafter, hydrogen and apolar bonds between the C1 and C2 domains reinforce the formation of the dimeric bouquet. In circulation at physiological pH of 7.4, shear forces of ≅50 pN can dissociate the stem of the dimeric bouquet.[48,49] However, the 2 parts of the bouquet are still covalently connected through cysteines so that the dimer roughly doubles its length and allows VWF multimer stretching. During this conformational transition, the D′D3 domain, which shields the A1 domain under static conditions, undergoes a structural change, exposing the GpIbα-binding site in the A1 domain and the Y1605-M1606 peptide bond proteolyzed by ADAMTS-13 in the A2 domain.[48] Noticeably, an anti-VWF monoclonal antibody (1C1E7) that recognizes an epitope in the 764- to 1035-aa region at the N-terminal D′D3 domains enhances VWF/GPIbα binding, proving that the D′D3 region of VWF negatively modulates VWF/GPIb-IX-V interaction[50] under static conditions. Hence, it is likely that the drastic changes of polarity and charge associated with the p.R924Q and p.A2178S mutations *in cis* may cooperatively alter the early steps of the conformational changes described earlier in this paragraph. The steric and polarity changes caused by these mutations, as shown by the results obtained by molecular modeling, favor the transition to a stretched conformation of VWF at shear forces lower than those needed for the WT VWF molecule, as previously observed in a canonical type 2B VWD.[21] The use of TEM and AFM techniques has shown that the heterozygous *in cis* mutations can indeed promote the transition toward an open/stretched conformational state of the VWF variant even in the virtual absence of shear forces. Likewise, lower than expected concentrations of ristocetin, whose binding to the A1 domain of VWF causes the same functional effects of mechanical forces,[49,51-53] were demonstrated to favor the interaction of the VWF variant to the platelet receptor, causing transient thrombocytopenia. In canonical forms of type 2B VWD, thrombocytopenia can be only transiently present and therefore sometimes not identified among the diagnostic criteria of type 2B VWD. In the pathological analysis of the propositus, thrombocytopenia was inconstant and mainly associated with stressful conditions, infections, and surgery, as previously reported in type 2B VWD.[8] In conclusion, this form of VWD differs from the canonical type 2B VWD forms as to the localization of causative genetic mutations, present *in cis* in the D′D3 and D4 domains. This scenario could suggest the existence of a novel subtype of 2B VWD that could be defined as type $2B^{D3D4}$. The results of this study show how genetic mutations occurring in the D′D3/D4 VWF domains may affect the conformational equilibria

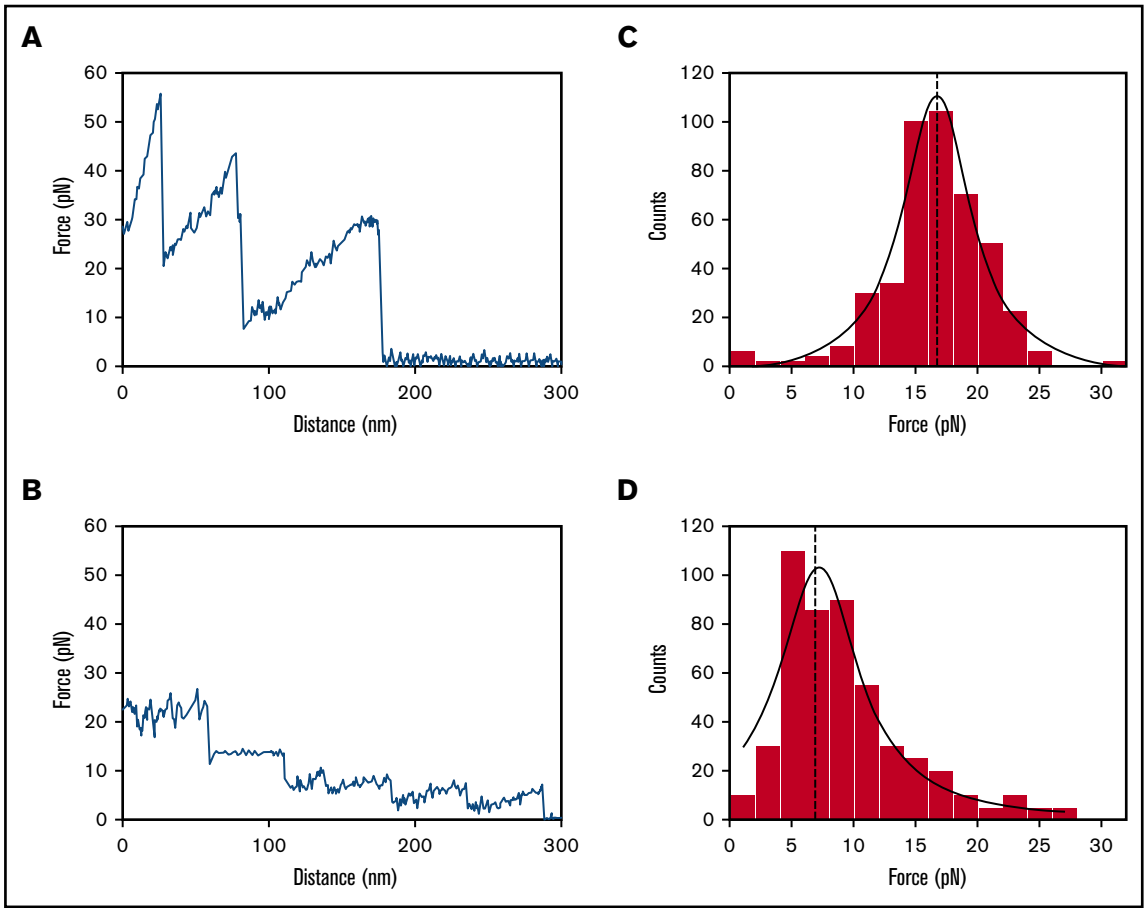

Figure 6. Force-extension assay of recombinant VWF forms using AFM. (A) The force-extension curve shows a saw-tooth pattern[54] for the WT form. (B) The heterozygous *in cis* mutant shows a much flatter profile. The microscope probe consisted of an ultrasharp silicon nitride cantilever of nominal force constant k = 0.1 N/m, with a tip radius of <10 nm (MikroMasch NSC16; NanoWorld, Neuchâtel, Switzerland). Image analysis was performed using Gwyddion software (Czech Metrology Institute, Brno, Czech Republic). (B) The force-extension curve concerning the *in cis* heterozygous form shows constant force plateaus, which are the expression of the mechanical unzipping of linear interactions between multiple linear polymer chains.[55] (C) Statistical analysis of the experimental data showed that the WT form has a median unfolding force of ~17 pN in good agreement with the average VWF unfolding force value previously reported.[21] (D) The *in cis* heterozygous form has an average unfolding force of ~7 pN. These unfolding force profiles agree with the morphological counterparts (Figure 5).

of mature VWF multimers, causing the expression of a 2B-like VWD phenotype. The rapid evolution of genetic and biochemical/biophysical techniques together with the development of new treatments may significantly change diagnostic flowcharts for VWD and their use for specific and personalized treatment.

Acknowledgments

R.D.C. gratefully acknowledges Maria Adele Alberelli for help in analyzing experimental data of platelet aggregation and acknowledges Franziska M. Lohmeyer (Fondazione Policlinico Universitario A. Gemelli, IRCCS, Rome, Italy) for accurate editing of the manuscript.

This work was supported by the University of the Sacred Heart, School of Medicine, Rome, Italy (Linea D1, AA 2018) (R.D.C.).

Authorship

Contribution: M.S., S.L., and M.T. performed all proteomic analyses; M. Papi and G.P. performed TEM and AFM experiments; F.B., M. Pinotti, M.F., and M.S. performed expression of recombinant VWF constructs; E.D.C., L.D.G., and M.B. performed clinical visits and follow-up of the patient; B.G. and G.C. conducted molecular genetics studies; R.D.C. designed the study, analyzed data, performed molecular modeling analyses, and wrote the manuscript; and all authors reviewed the manuscript.

Conflict-of-interest disclosure: The authors declare no competing financial interests.

ORCID profiles: M.F., 0000-0001-7827-9249; F.B., 0000-0003-0305-2212; E.D.C., 0000-0003-0942-2819; M. Papi, 0000-0002-0029-1309; G.P., 0000-0001-9452-8479; R.D.C., 0000-0002-8066-8849.

Correspondence: Raimondo De Cristofaro, Università Cattolica S. Cuore–Facoltà di Medicina e Chirurgia–Fondazione Policlinico Universitario A. Gemelli IRCCS, Largo F. Vito, 1, 00168 Rome, Italy; e-mail: raimondo.decristofaro@unicatt.it.

References

1. Meyer D, Girma JP. von Willebrand factor: structure and function. *Thromb Haemost*. 1993;70(1):99-104.
2. Mancuso DJ, Tuley EA, Westfield LA, et al. Structure of the gene for human von Willebrand factor. *J Biol Chem*. 1989;264(33):19514-19527.
3. Titani K, Kumar S, Takio K, et al. Amino acid sequence of human von Willebrand factor. *Biochemistry*. 1986;25(11):3171-3184.
4. Sadler JE. Biochemistry and genetics of von Willebrand factor. *Annu Rev Biochem*. 1998;67:395-424.
5. Zhou YF, Eng ET, Zhu J, Lu C, Walz T, Springer TA. Sequence and structure relationships within von Willebrand factor. *Blood*. 2012;120(2):449-458.
6. Keesler DA, Flood VH. Current issues in diagnosis and treatment of von Willebrand disease. *Res Pract Thromb Haemost*. 2017;2(1):34-41.
7. Sadler JE, Budde U, Eikenboom JC, et al; Working Party on von Willebrand Disease Classification. Update on the pathophysiology and classification of von Willebrand disease: a report of the subcommittee on von Willebrand factor. *J Thromb Haemost*. 2006;4(10):2103-2114.
8. Federici AB, Mannucci PM, Castaman G, et al. Clinical and molecular predictors of thrombocytopenia and risk of bleeding in patients with von Willebrand disease type 2B: a cohort study of 67 patients. *Blood*. 2009;113(3):526-534.
9. Peerlinck K, Eikenboom JC, Ploos Van Amstel HK, et al. A patient with von Willebrand's disease characterized by a compound heterozygosity for a substitution of Arg854 by Gln in the putative factor-VIII-binding domain of von Willebrand factor (vWF) on one allele and very low levels of mRNA from the second vWF allele. *Br J Haematol*. 1992;80(3):358-363.
10. Siguret V, Lavergne JM, Chérel G, et al. A novel case of compound heterozygosity with "Normandy"/type I von Willebrand disease (vWD). Direct demonstration of the segregation of one allele with a defective expression at the mRNA level causing type I vWD. *Hum Genet*. 1994;93(2):95-102.
11. Kroner PA, Foster PA, Fahs SA, Montgomery RR. The defective interaction between von Willebrand factor and factor VIII in a patient with type 1 von Willebrand disease is caused by substitution of Arg19 and His54 in mature von Willebrand factor. *Blood*. 1996;87(3):1013-1021.
12. Ribba AS, Lavergne JM, Bahnak BR, Derlon A, Piétu G, Meyer D. Duplication of a methionine within the glycoprotein Ib binding domain of von Willebrand factor detected by denaturing gradient gel electrophoresis in a patient with type IIB von Willebrand disease. *Blood*. 1991;78(7):1738-1743.
13. Michiels JJ, Berneman Z, Gadisseur A, et al. Classification and characterization of hereditary types 2A, 2B, 2C, 2D, 2E, 2M, 2N, and 2U (unclassifiable) von Willebrand disease. *Clin Appl Thromb Hemost*. 2006;12(4):397-420.
14. Rodeghiero F, Tosetto A, Abshire T, et al; ISTH/SSC joint VWF and Perinatal/Pediatric Hemostasis Subcommittees Working Group. ISTH/SSC bleeding assessment tool: a standardized questionnaire and a proposal for a new bleeding score for inherited bleeding disorders. *J Thromb Haemost*. 2010;8(9):2063-2065.
15. de Maistre E, Volot F, Mourey G, et al. Performance of two new automated assays for measuring von Willebrand activity: HemosIL AcuStar and Innovance. *Thromb Haemost*. 2014;112(4):825-830.
16. Costa-Pinto J, Pérez-Rodríguez A, del C Goméz-del-Castillo M, et al. Diagnosis of inherited von Willebrand disease: comparison of two methodologies and analysis of the discrepancies. *Haemophilia*. 2014;20(4):559-567.
17. Veyradier A, Caron C, Ternisien C, et al. Validation of the first commercial ELISA for type 2N von Willebrand's disease diagnosis. *Haemophilia*. 2011; 17(6):944-951.
18. Tiede A, Priesack J, Werwitzke S, et al. Diagnostic workup of patients with acquired von Willebrand syndrome: a retrospective single-centre cohort study. *J Thromb Haemost*. 2008;6(4):569-576.
19. Haberichter SL, Balistreri M, Christopherson P, et al. Assay of the von Willebrand factor (VWF) propeptide to identify patients with type 1 von Willebrand disease with decreased VWF survival. *Blood*. 2006;108(10):3344-3351.
20. Lancellotti S, Peyvandi F, Pagliari MT, et al. The D173G mutation in ADAMTS-13 causes a severe form of congenital thrombotic thrombocytopenic purpura. A clinical, biochemical and in silico study. *Thromb Haemost*. 2016;115(1):51-62.
21. Scaglione GL, Lancellotti S, Papi M, et al. The type 2B p.R1306W natural mutation of von Willebrand factor dramatically enhances the multimer sensitivity to shear stress. *J Thromb Haemost*. 2013;11(9):1688-1698.
22. Othman M, Kaur H, Favaloro EJ, et al; Subcommittees on von Willebrand Disease and Platelet Physiology. Platelet type von Willebrand disease and registry report: communication from the SSC of the ISTH. *J Thromb Haemost*. 2016;14(2):411-414.
23. Morling N, Allen RW, Carracedo A, et al; Paternity Testing Commission of the International Society of Forensic Genetics. Paternity Testing Commission of the International Society of Forensic Genetics: recommendations on genetic investigations in paternity cases. *Forensic Sci Int*. 2002;129(3):148-157.
24. Casari C, Pinotti M, Lancellotti S, et al. The dominant-negative von Willebrand factor gene deletion p.P1127_C1948delinsR: molecular mechanism and modulation. *Blood*. 2010;116(24):5371-5376.
25. Wu S, Skolnick J, Zhang Y. Ab initio modeling of small proteins by iterative TASSER simulations. *BMC Biol*. 2007;5(1):17.
26. Zhang Y. Template-based modeling and free modeling by I-TASSER in CASP7. *Proteins*. 2007;69(suppl 8):108-117.
27. Papi M, Maulucci G, De Spirito M, et al. Ristocetin-induced self-aggregation of von Willebrand factor. *Eur Biophys J*. 2010;39(12):1597-1603.
28. Brunelli R, Papi M, Arcovito G, et al. Globular structure of human ovulatory cervical mucus. *FASEB J*. 2007;21(14):3872-3876.
29. Hickson N, Hampshire D, Winship P, et al; MCMDM-1VWD and ZPMCB-VWD study groups. von Willebrand factor variant p.Arg924Gln marks an allele associated with reduced von Willebrand factor and factor VIII levels. *J Thromb Haemost*. 2010;8(9):1986-1993.
30. Lester W, Guilliatt A, Grundy P, et al. Is VWF R924Q a benign polymorphism, a marker of a null allele or a factor VIII-binding defect? The debate continues with results from the UKHCDO VWD study. *Thromb Haemost*. 2008;100(4):716-718.

31. Berber E, James PD, Hough C, Lillicrap D. An assessment of the pathogenic significance of the R924Q von Willebrand factor substitution. *J Thromb Haemost*. 2009;7(10):1672-1679.

32. Hilbert L, Jorieux S, Proulle V, et al; INSERM Network on Molecular Abnormalities in von Willebrand Disease. Two novel mutations, Q1053H and C1060R, located in the D3 domain of von Willebrand factor, are responsible for decreased FVIII-binding capacity. *Br J Haematol*. 2003;120(4):627-632.

33. Cumming A, Grundy P, Keeney S, et al; UK Haemophilia Centre Doctors' Organisation. An investigation of the von Willebrand factor genotype in UK patients diagnosed to have type 1 von Willebrand disease. *Thromb Haemost*. 2006;96(5):630-641.

34. Xu D, Zhang J, Roy A, Zhang Y. Automated protein structure modeling in CASP9 by I-TASSER pipeline combined with QUARK-based ab initio folding and FG-MD-based structure refinement. *Proteins*. 2011;79(suppl 10):147-160.

35. Zhang Y. Interplay of I-TASSER and QUARK for template-based and ab initio protein structure prediction in CASP10. *Proteins*. 2014;82(suppl 2): 175-187.

36. Yang J, Wang Y, Zhang Y. ResQ: an approach to unified estimation of B-factor and residue-specific error in protein structure prediction. *J Mol Biol*. 2016; 428(4):693-701.

37. Rounsevell RW, Steward A, Clarke J. Biophysical investigations of engineered polyproteins: implications for force data. *Biophys J*. 2005;88(3): 2022-2029.

38. Fisher TE, Marszalek PE, Oberhauser AF, Carrion-Vazquez M, Fernandez JM. The micro-mechanics of single molecules studied with atomic force microscopy. *J Physiol*. 1999;520(pt 1):5-14.

39. McGinnis E, Vercauteren SM. von Willebrand disease type 2B. *Blood*. 2016;128(23):2743.

40. Shim K, Anderson PJ, Tuley EA, Wiswall E, Sadler JE. Platelet-VWF complexes are preferred substrates of ADAMTS13 under fluid shear stress. *Blood*. 2008;111(2):651-657.

41. Schneider SW, Nuschele S, Wixforth A, et al. Shear-induced unfolding triggers adhesion of von Willebrand factor fibers. *Proc Natl Acad Sci USA*. 2007; 104(19):7899-7903.

42. Ruggeri ZM, Orje JN, Habermann R, Federici AB, Reininger AJ. Activation-independent platelet adhesion and aggregation under elevated shear stress. *Blood*. 2006;108(6):1903-1910.

43. Borchiellini A, Fijnvandraat K, ten Cate JW, et al. Quantitative analysis of von Willebrand factor propeptide release in vivo: effect of experimental endotoxemia and administration of 1-deamino-8-D-arginine vasopressin in humans. *Blood*. 1996;88(8):2951-2958.

44. Goodeve A. Diagnosing von Willebrand disease: genetic analysis. *Hematology Am Soc Hematol Educ Program*. 2016;2016:678-682.

45. Katsumi A, Tuley EA, Bodó I, Sadler JE. Localization of disulfide bonds in the cystine knot domain of human von Willebrand factor. *J Biol Chem*. 2000; 275(33):25585-25594.

46. Huang RH, Wang Y, Roth R, et al. Assembly of Weibel-Palade body-like tubules from N-terminal domains of von Willebrand factor. *Proc Natl Acad Sci USA*. 2008;105(2):482-487.

47. Zhou YF, Springer TA. Highly reinforced structure of a C-terminal dimerization domain in von Willebrand factor. *Blood*. 2014;123(12):1785-1793.

48. Zhou YF, Eng ET, Nishida N, Lu C, Walz T, Springer TA. A pH-regulated dimeric bouquet in the structure of von Willebrand factor. *EMBO J*. 2011;30(19): 4098-4111.

49. Lancellotti S, Sacco M, Basso M, De Cristofaro R. Mechanochemistry of von Willebrand factor. *Biomol Concepts*. 2019;10(1):194-208.

50. Ulrichts H, Udvardy M, Lenting PJ, et al. Shielding of the A1 domain by the D′D3 domains of von Willebrand factor modulates its interaction with platelet glycoprotein Ib-IX-V. *J Biol Chem*. 2006;281(8):4699-4707.

51. Hoylaerts MF, Nuyts K, Peerlinck K, Deckmyn H, Vermylen J. Promotion of binding of von Willebrand factor to platelet glycoprotein Ib by dimers of ristocetin. *Biochem J*. 1995;306(pt 2):453-463.

52. Di Stasio E, Romitelli F, Lancellotti S, Arcovito A, Giardina B, De Cristofaro R. Kinetic study of von Willebrand factor self-aggregation induced by ristocetin. *Biophys Chem*. 2009;144(3):101-107.

53. Chen J, Ling M, Fu X, López JA, Chung DW. Simultaneous exposure of sites in von Willebrand factor for glycoprotein Ib binding and ADAMTS13 cleavage: studies with ristocetin. *Arterioscler Thromb Vasc Biol*. 2012;32(11):2625-2630.

54. Wijeratne SS, Li J, Yeh HC, et al. Single-molecule force measurements of the polymerizing dimeric subunit of von Willebrand factor. *Phys Rev E*. 2016; 93(1):012410.

55. Alsteens D, Martinez N, Jamin M, Jacob-Dubuisson F. Sequential unfolding of beta helical protein by single-molecule atomic force microscopy. *PLoS One*. 2013;8(8):e73572.